Earthquake Engineering, Tenth World Conference © 1992 Balkema, Rotterdam. ISBN 90 5410 060 5

Attenuation of shear waves in a sediment

Shigeo Kinoshita
National Research Institute for Earth Science and Disaster Prevention, Tsukuba, Japan

ABSTRACT: We determined $1/Q(\omega)$ for shear waves in a sedimentary layers - basement system assuming all layers, including the basement, have the same attenuation characteristics. The determination of $1/Q(\omega)$ is based on a comparative study of the amplification function of the system and its estimate which is valued by using the strong motion data obtained by means of borehole array observation including a deep borehole with a depth of 2.3 km. To this end, we selected three kinds of the amplification function of the system. Although there is a rough handling of $1/Q(\omega)$, the results of our estimation indicated the following frequency dependence, *i.e.*, $1/Q(\omega)$ is about 0.01 in frequencies higher than 5 Hz and is proportional to $f^{-(0.5\sim0.6)}$ in a frequency range between 0.2 and 4 Hz.

1 INTRODUCTION

The importance of site effects for the critical study of both the path effects and source characteristics has been recognized during the last decade. From the viewpoint of earthquake engineering, the site effects of various types of the sedimentary layer for shear waves have been investigated by many researchers. However, much information on shear waves attenuation in sedimentary layers has yet to be obtained.

A reasonable idea for the estimation of the shear waves attenuation is to recognize the input waves in the basement and the output ones of the sedimentary layers by installing seismometers in both the basement and the sedimentary layers, respectively. Borehole observation that realizes this idea has progressed much in the last decade. The most critical problem of the borehole method is that the response of a sedimentary layers - basement system is a response of the feedback system. A countermeasure against the input wave reverberated with downgoing noises must be taken into account for the estimation of attenuation characteristics.

In this study, we will show evidence that shear wave attenuation in a sedimentary layer - basement system depends on frequency, by making a comparative study between the target function, *i.e.*, the amplification function of the system and its estimate obtained from actual strong motion data accumulated by means of borehole array observation. Three target functions G_n, n=1,2,3 are selected for that purpose. The method using G_1 is closely associated with a skill to weaken the feedback effects in a high frequency band by using two boreholes in the same station. Another method using G_2 is an active application of the feedback effect by using a deep borehole. This method has an advantage of using only one seismometer, which is commonly required in the ideal source-canceling method. G_3 is the most standard function in such a work. The seismic records obtained simultaneously both on a free surface and at the bottom of a deep borehole are applied to this target function.

2 METHODS

In this section, the z-transform representation of target functions used in our estimation scheme is specifically described. In this paper, z^{-1} is defined as follows:

$$z^{-1} = \exp(-i\lambda), \quad \lambda = \omega \cdot \Delta T,$$

where $\lambda, (-\pi \le \lambda \le \pi)$ is a normalized angular frequency and ΔT is the sampling time. A straightforward scheme for the estimation of $1/Q(\omega)$ from borehole seismic data is completed in a series of three steps. The first step is the selection of a target function $G(\lambda)$. Spectral analysis to obtain an estimate $\hat{G}(\lambda)$ of $G(\lambda)$, by applying it to actual seismic data, is the next step. An application of a frequency transform to $G(\lambda)$ to evaluate $1/Q(\omega)$ is the final step. To do this, a special case where the type of viscoelasticity is common to all layers including the basement layer is considered. Then, the frequency transform is as follows:

$$\lambda \to \lambda(1 + i/Q(\omega))^{-1/2}$$
$$\sim \lambda - i\lambda/2Q(\omega), \quad Q(\omega) \gg 1.$$

When using the z-transform representation of $G(\lambda)$, this change of the frequency parameter λ converts z^{-1} in $G(\lambda)$ into $\exp(-\lambda/2Q(\omega))\cdot z^{-1}$. This means that all layers have equal attenuation characteristics. Although our introduction of $1/Q(\omega)$ is very simple, it seems to be enough for an estimate of the average $1/Q(\omega)$ in a sedimentary layers - basement system.

A specific case is considered where two seismometers, S_i and S_o, are installed as shown in Fig.1. One seismometer (S_i) is fixed in the basement and the other (S_o) is controlled by the depth level and is installed in the sedimentary layers or in the basement. The target function $G(\lambda)$ is defined by the amplitude ratio of the Fourier transform of the SH-wave recorded by S_o to that by S_i. A usual choice for selecting $G(\lambda)$ is to install S_o on a free surface, though it is not the best choice for the estimation of $1/Q(\omega)$. In the case where S_o is located on a free surface, $G(\lambda)$ has the structure of a narrowband filter, and it is too sensitive to a change of $1/Q(\omega)$. We denote this target function as $G_3(\lambda)$. As the depth level of the location of S_o increases, the poles of $G(\lambda)$ in a high frequency region are approximately cancelled by the zeros of $G(\lambda)$. Namely, $G(\lambda)$ has the characteristics of a constant filter in a high frequency region, and is robust to a change of $1/Q(\omega)$. One strategy for getting suitable target functions apart from the standard choice is to install S_o at any given depth level, so that $G(\lambda)$ moves from a narrowband structure to a constant structure in a frequency band for the estimation of $1/Q(\omega)$. This strategy has an essential effect in a seismological aspect, *i.e.*, the suppression of the energy power of Love waves on the recorded seismograms by S_o. In this paper, we denote such a type of target function as $G_1(\lambda)$.

For the next strategy of getting another target function, the depth level of S_o is increased further. When $S_o = S_i$, $G(\lambda)$ becomes the unity for all λ. In this self-evident situation, the definition of $G(\lambda)$ has to be modified in order to succeed in the evaluation of $1/Q(\omega)$. From the standpoint of the source-canceling method for the estimation of $1/Q(\omega)$, it is reasonable to turn attention to the separation of the SH-waves detected by $S_o(=S_i)$ into the incident waves in the basement and the reflected waves from the sedimentary layers, which have Fourier transform $\overline{X}(\lambda)$ and $\underline{X}(\lambda)$, respectively. The Fourier ratio of observed waves, $(\overline{X}(\lambda)+\underline{X}(\lambda))$, to unknown incident waves, $\overline{X}(\lambda)$, is represented as follows:

$$(\overline{X}(\lambda)+\underline{X}(\lambda))/\overline{X}(\lambda) = 1+\underline{X}(\lambda)/\overline{X}(\lambda)$$

The left hand side of the above relation is a notch filter, and a minimum phase function. On the contrary, the second term of the right hand side of this relation is an all-pass filter. The numerator, $\underline{X}(\lambda)$, has zeros outside the unit circle in the z^{-1}-plane and is not a minimum phase function, although $\overline{X}(\lambda)/\underline{X}(\lambda)$ is a one-sided (causal) function of time. This is due to the fact that each pair of a zero and a pole is on the same radius line in the z^{-1}-plane and the product is unity. Then $\overline{X}(\lambda)/\underline{X}(\lambda)$ is a target function $G(\lambda)$, if $\overline{X}(\lambda)$ and $\underline{X}(\lambda)$ are observed separately enough on the time axis. This condition is approximately attainable when the location of $S_i(=S_o)$ is so deep that the main reverberation energy from the sedimentary layers and free surface is delayed long enough. We denote such a target function as $G_2(\lambda)$. In actual data processing, $G_2(\lambda)$ is defined by using an impulse response of $1+\overline{X}(\lambda)/\underline{X}(\lambda)$. Since the target function is a one-sided function and has a rational expression of z^{-1}, it is easy to calculate its impulse response. The length of data used for the estimation of $G(\lambda)$ is not infinite. Using the data length of $N\cdot\Delta T$, a truncated impulse response corresponds to the target function. From this point, $G(\lambda)$ will be treated as such a transient function, though it has been discussed up to here as a stationary one. The rough evaluation of $1/Q(\omega)$ is obtained to make a comparison between a target function $G(\lambda)$ and its estimate $\hat{G}(\lambda)$.

When considering the response of a sedimentary layers - basement system in order to estimate $1/Q(\omega)$ in the system, that of a multi-layered half space for obliquely incidental SH-waves seems to be a non-problematical approximation. Thus we will consider the Goupillaud model with p+1 layers and will assume that two seismometers, So and Si, are installed in the (k+1)th and the (p+1)th layers, respectively, as shown in Fig.1. The impedance in the k-th layer is $\alpha_k = \rho_k\beta_k\cos\theta_k, (1\le k\le p+1 \text{ and } \alpha_0 = 0)$, where ρ_k, β_k and θ_k are density, shear wave velocity and the angle of incidence in the k-th layer, respectively. Then from the definition of reflection coefficients:

$$\gamma_{k+1} = (\alpha_{k+1}-\alpha_k)/(\alpha_{k+1}+\alpha_k), \quad (0\le k\le p),$$

and the Durbin - Levinson recursion:

$$g_{k,k} = \gamma_k, \quad (1\le k\le p)$$

and

$$g_{k,n} = g_{k-1,n} + g_{k,k}g_{k-1,k-n}, \quad (1\le n\le k-1),$$

we obtain a target function, *i.e.*, $G_1(\lambda)$,

$$\frac{\overline{X}_{k+1}(\lambda)+\underline{X}_{k+1}(\lambda)}{\overline{X}_{p+1}(\lambda)+\underline{X}_{p+1}(\lambda)} = \left(\frac{\sigma_p}{\sigma_k}\right)\cdot z^{-(p-k)/2}\cdot\frac{\sum_{n=0}^{k} g_n^{(k)} z^{-n}}{\sum_{n=0}^{p} g_n^{(p)} z^{-n}}, \qquad (1)$$

where $g_{k,0} = 1, \ (1\le k\le p)$,

$$g_n^{(k)} = \frac{(g_{k,n} + g_{k,k-n})}{(g_{k,0} + g_{k,k})}, \quad (1 \le k \le p, 1 \le n \le k),$$

and

$$\sigma_k = \sum_{n=0}^{p} g_n^{(k)}, \quad (1 \le k \le p).$$

In the left-hand side of the target function (1), $\overline{X}_{k+1}(\lambda)$ and $\underline{X}_{k+1}(\lambda)$ represent the Fourier transforms of the upgoing and downgoing waves, respectively, in the (k+1)th layer.

When *So* is installed on a free surface, the system function has the following form:

$$\frac{\sigma_p z^{-p/2}}{\sum_{n=0}^{p} g_n^{(p)} z^{-n}}. \qquad (2)$$

The amplification function of this system function is used as the most standard target function, *i.e.* $G_3(\lambda)$.

When $S_o(=S_1)$, the system function of SH-waves recorded in the basement, *i.e.*, (p+1)th layer, to the unknown upgoing SH-waves is as follows:

$$1 + \frac{\underline{X}_{p+1}(\lambda)}{\overline{X}_{p+1}(\lambda)} = 1 + \frac{\sum_{n=0}^{p} g_{p,p-n} z^{-n}}{\sum_{n=0}^{p} g_{p,n} z^{-n}}. \qquad (3)$$

In section 4, a target function $G_2(\lambda)$ is constructed by making use of the impulse response of the system function (3).

3 DATA

The data used for the estimation of $1/Q(\omega)$ are acceleration records obtained at the Shimohsa crustal activity observatory (SHM) in the Kanto area, Japan. At the SHM site a force - balanced tri-axial accelerometer is installed at three different depth levels, *i.e.*, free surface (one meter depth), 200 m and 2.3 km. The natural frequency and damping factor of this type of accelerometer are about 450 Hz and 0.6, respectively. Acceleration signals from these seismometers are recorded digitally on magnetic tape with a digitization rate of 100 Hz. The over-all data acquisition system including the accelerometer has flat response characteristics from DC to a cutoff frequency of 30 Hz.

In this study, three sets of acceleration data were selected. The earthquakes in these data sets are tabulated and shown in Table 1. In the study on $1/Q(\omega)$, the velocity structure of a sedimentary layers - basement system in the site was needed. The structure of the shear wave velocity, density and layer thickness in the SHM site have already been investigated and tabulated as shown in Table 2.

4 RESULTS

The target function $G_1(\lambda)$ is defined in this site as the amplification factor of SH-waves at a depth of 200 meters to those at a depth of 2300 meters. The spectral ratio $\hat{G}_1(\lambda)$ is estimated by applying the multitaper method to the transverse component records of direct S waves with a time length of 2.56 seconds obtained at each depth of the well. The bandwidth $2W$ of the multitaper spectral estimation is determined by $2P/N \cdot \Delta T$. N is the total number of samples and parameter P controls the shapes of the data window. For the estimation of $\hat{G}_1(\lambda)$, we used P=4, *i.e.*, $2W$=3.125 Hz. This choice of $2W$ is due to the fact the magnitude range of earthquakes is from 3.5 to 6.0 on the JMA scale so that the predominant frequency band of the input acceleration spectrum is higher than $2W$. Fig.3(a) shows the six lowest-order data windows, which correspond to the six lowest-order eigenvectors. Fig.4 shows the average spectral windows calculated from all data windows shown in Fig.3(a).

From a data set of 30 events which are indicated by category "1" in Table 1, the average $\hat{G}_1(\lambda)$ (solid line) is estimated as shown in Fig.5. Two dashed lines in this figure indicate one standard error range. Our objective is to obtain $1/Q(\omega)$, by which $G_1(\lambda)$ agrees with $\hat{G}_1(\lambda)$ as a result. The calculation of $G_1(\lambda)$ needs two parameters, $1/Q(\omega)$ and an incidence angle of input SH-waves in the basement. Bold line $G_1(\lambda)$, calculated assuming $1/Q(\omega) = 1/110$ and an incidence angle of 30 ° , as shown in Fig.5, shows the best fitting. $G_1(\lambda)$ in frequencies higher than 5 Hz is almost independent of the angle of the incidence because of strong attenuation of SH-waves, i.e., $1/Q(\omega) \sim 1/110$.

The next method, which uses the target function $G_2(\lambda)$ for estimation of $1/Q(\omega)$ is applied to the data from ten events which are indicated by category "2", as shown in Table 1. This method use the spectral ratio calculated from two time series in two segments, which are determined by the following procedure, on the same seismogram recorded at the bottom of the 2.3 km hole. Fig.6 illustrates the procedure for picking up these two segments by the using transverse component record obtained on April 1, 1988. We first applied a band-pass filtering to the transverse component seismogram $\{x(n)\}$ between 0.8 and 5.0 Hz, using a phaseless two poles filter. Next, we determined the acceleration envelope $e(n)$ from $e(n) = \{b^2(n) + H^2\{b(n)\}\}^{1/2}$, where $b(n)$ is the band-passed time series and $H\{b(n)\}$ is its Hilbert transform. In general, the acceleration envelope $e(n)$ builds up from the onset of direct S-waves and abates with the end of its energy arrival. Such an energy packet is reproduced on the same envelope function of time, because of the total reflection of the direct wave at

the free surface. Two segments denoted by B_l and B_r in Fig.6 show this fact. Our procedure to determine B_l and B_r is very simple. B_l with a time length of $(2M+1)\cdot\Delta T$ is determined visually. In order to determine the segment B_r, we first calculate the cross correlation function of two band-pass trains, which are in the segment B_l and in a tentative segment including surface reflected waves, and then select a segment B_r having the maximum cross correlation from a set of tentative segments. After determining the two segments, calculation of the spectral ratio is made for comparison with target function $G_2(\lambda)$:

$$G_2(\lambda) = \frac{z^{-p}\sum_{m=-M}^{M} h_{m+p}\cdot z^{-m}}{1+\sum_{m=0}^{M} h_m\cdot z^{-m}}, \qquad (4)$$

where $\{h_m\}_{m=0}^{\infty}$ is an impulse response of $\underline{X}_{p+1}(\lambda)/\overline{X}_{p+1}(\lambda)$. An incident angle of impulse in the basement is needed for calculation of the impulse response. This angle is determined from the delay time t_d of the surface reflected wave to its direct one in the basement. For our data set, $t_d = 4.88\pm0.06\,(s)$ is obtained. This delay time corresponds to the incident angle of $30\pm6°$. Fig.7 shows an impulse response with an incident angle of 30° . Four data windows shown in Fig.3(b) were calculated with P=2.56 and N=256, and then applied to the data of two segments to obtain the Fourier spectrum. The dashed line in Fig.4 is the corresponding average spectral window with a bandwidth $2W$=2 Hz. The estimated spectral ratio (solid circles) and a target function (bold line) are shown in Fig.8. The results indicate that $1/Q(\omega) = 1/80f^{0.6}$ is the best.

To further investigate the frequency dependence of $1/Q(\omega)$ in frequencies less than 1 Hz, we have to deal with strong motion data offered from larger events than those used thus far. Thus, we examined the data simultaneously recorded at the bottom of the deepest well and on the free surface in the SHM site. Six events listed as category "3" in Table 1 have a magnitude range between 6.0 and 7.0, and the data from these events were studied by making use of a target function $G_3(\lambda)$ as defined by function (2). There is a condition which is indispensable to select the events and is needed to handle $G_3(\lambda)$ as the target function. The cross correlation function, which is calculated from two time series recorded at the free surface and the bottom of a well, is to be a nearly even function with the extreme at two points corresponding to the one-way time between two seismometers. This condition of the cross correlation function is easily derived from $G_3(\lambda)$ as defined by function (2), and it is a useful basis to understand the events having low level energy of Love waves. Transverse components with a duration of 20 seconds (25 seconds only for the No.2 event in Table 1), are used for the calculation of $\hat{G}_3(\lambda)$. In Fig.9, $\hat{G}_3(\lambda)$ (dashed line) and two kinds of $G_3(\lambda)$ (real lines) calculated under the same angle of incidence are shown. The incident angle of input SH-waves in the basement is 30° and two $1/Q(\omega)$'s , *i.e.*, 1/110 and $1/60f^{0.5}$, make the difference between two real lines.

5 CONCLUSION

Assuming all layers including the basement layer have the same attenuation characteristics, we determined $1/Q(\omega)$ for S-waves in a sedimentary layers - basement system in the Kanto area, Japan. Although there was a rough handling of $1/Q(\omega)$, our study yielded the following results:
$1/Q(\omega)$ is almost constant, *i.e.*, 1/110 in frequencies higher than 5 Hz. On the other hand, frequency dependence of $1/Q(\omega)$ is apparent in a frequency range between 0.2 and 4 Hz and is proportional to $f^{-(0.5-0.6)}$.

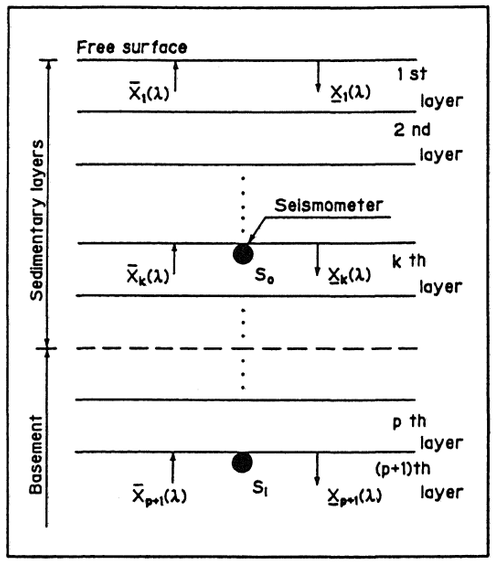

Figure 1. The equal time layered model for calculation of response functions of a sedimentary layers - basement system. One seismometer, S_l ,is fixed in the basement and the depth level of the other seismometer, S_0 , is controlled to obtain the output of various types of the response function.

Table 1. List of earthquakes used in the determination of $1/Q(\omega)$ from the SHM array records.

NO.	Year	Date D	M	H	M	Latitude	Longitude	Depth (km)	M_{JMA}	Category
1	1980	24	09	04	10	35° 58′ 00″ N	139° 48′ 06″ E	80.0	5.4	2
2	1982	23	07	23	23	36° 11′ 06″ N	141° 57′ 12″ E	30.0	7.0	3
3	1984	17	12	14	55	35° 57′ 54″ N	140° 05′ 12″ E	72.0	4.2	2
4	1985	08	06	01	29	35° 32′ 18″ N	140° 14′ 54″ E	64.0	4.8	2
5	1985	04	10	21	25	35° 52′ 06″ N	140° 09′ 30″ E	78.0	6.1	2 , 3
6	1986	24	06	11	53	34° 49′ 24″ N	140° 43′ 12″ E	73.0	6.5	3
7	1987	11	06	16	00	36° 10′ 48″ N	140° 02′ 54″ E	55.0	3.9	1
8	1987	16	06	00	30	35° 37′ 24″ N	140° 11′ 30″ E	75.7	4.4	2
9	1987	25	06	15	45	35° 41′ 06″ N	139° 41′ 24″ E	36.7	3.6	1
10	1987	30	06	18	17	36° 11′ 00″ N	140° 05′ 18″ E	56.5	4.9	1
11	1987	12	07	13	31	36° 08′ 42″ N	140° 03′ 36″ E	56.9	4.6	1
12	1987	17	12	11	08	35° 22′ 18″ N	140° 29′ 48″ E	57.9	6.7	3
13	1987	17	12	14	07	35° 23′ 36″ N	140° 29′ 06″ E	57.8	4.4	1
14	1988	05	01	10	09	35° 24′ 42″ N	140° 26′ 00″ E	42.0	4.2	1
15	1988	16	01	20	42	35° 23′ 12″ N	140° 24′ 48″ E	47.6	5.2	1 , 2
16	1988	17	01	01	19	35° 23′ 06″ N	140° 25′ 06″ E	44.8	3.9	1
17	1988	18	01	19	37	35° 33′ 12″ N	139° 56′ 36″ E	31.8	4.1	1
18	1988	25	02	17	06	35° 22′ 06″ N	140° 22′ 06″ E	37.9	4.1	1
19	1988	18	03	05	34	35° 39′ 42″ N	139° 38′ 48″ E	98.1	6.0	1 , 3
20	1988	01	04	07	22	35° 33′ 18″ N	140° 10′ 00″ E	74.9	4.6	1 , 2
21	1988	30	05	19	45	36° 27′ 36″ N	140° 42′ 12″ E	49.0	4.7	1
22	1988	15	07	03	17	35° 54′ 18″ N	140° 09′ 42″ E	75.7	4.2	1
23	1988	12	08	14	14	35° 05′ 42″ N	139° 52′ 00″ E	69.4	5.3	1
24	1988	05	09	00	49	35° 29′ 48″ N	138° 59′ 12″ E	29.8	5.6	1
25	1988	16	09	03	18	36° 12′ 00″ N	140° 04′ 00″ E	61.2	4.5	1
26	1988	26	09	17	23	35° 32′ 30″ N	141° 10′ 54″ E	35.7	5.8	1
27	1988	30	09	02	38	35° 56′ 24″ N	139° 11′ 12″ E	15.9	4.5	1
28	1988	31	10	01	25	36° 11′ 24″ N	140° 00′ 00″ E	58.9	3.9	1
29	1988	28	12	18	02	36° 04′ 06″ N	139° 55′ 06″ E	56.0	4.3	1
30	1989	19	02	21	27	36° 01′ 06″ N	139° 54′ 30″ E	55.3	5.6	1 , 2
31	1989	06	03	23	39	35° 41′ 30″ N	140° 42′ 32″ E	55.7	6.0	1 , 3
32	1989	11	03	16	12	35° 54′ 30″ N	140° 33′ 48″ E	44.6	4.9	1
33	1989	18	03	01	37	35° 43′ 54″ N	140° 43′ 42″ E	50.6	5.2	1
34	1989	26	04	02	18	35° 54′ 36″ N	140° 29′ 36″ E	64.8	5.4	1
35	1989	26	08	09	11	36° 16′ 00″ N	140° 56′ 42″ E	38.9	5.1	1
36	1989	05	09	13	07	35° 33′ 11″ N	140° 08′ 18″ E	78.2	4.6	1 , 2
37	1989	10	10	15	28	35° 34′ 54″ N	140° 03′ 30″ E	78.3	4.7	1
38	1989	14	10	06	19	34° 49′ 24″ N	139° 30′ 12″ E	21.2	5.7	1

Table 2. S-wave velocity structure at the SHM site.

Layer No.	V_s(km/s)	ρ(g/cm^3)	H(m)
1	0.17	1.7	3.
2	0.24	1.8	9.5
3	0.35	1.8	7.
4	0.41	1.9	12.5
5	0.33	1.9	16.5
6	0.27	1.8	2.5
7	0.35	1.9	28.
8	0.45	2.0	272.
9	0.72	2.1	497.
10	0.90	2.2	345.
11	1.17	2.5	309.
12	2.54	2.7	****

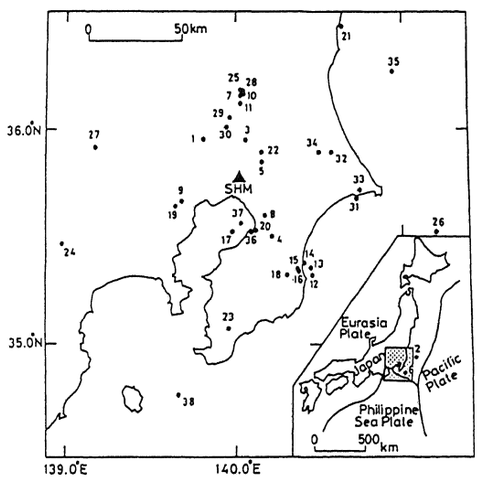

Figure 2. Epicenters of earthquakes used in the determination of $1/Q(\omega)$ from the SHM array records. Closed triangle represents the location of the SHM site (140° 01'25.6"E, 35° 47'36.4"N).

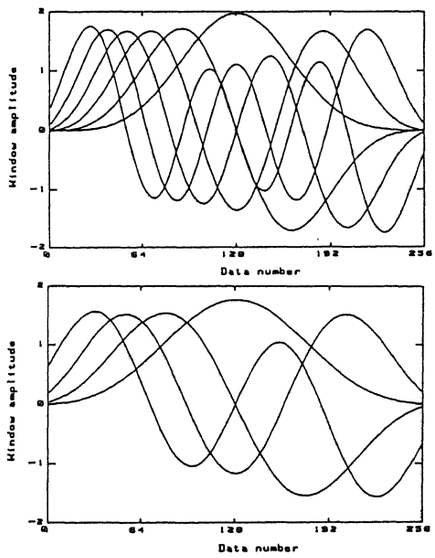

Figure 3. (a) The six lowest-order data windows for a duration time-bandwidth product of 4. (b) The four lowest-order data windows for a duration time-bandwidth product of 2.56.

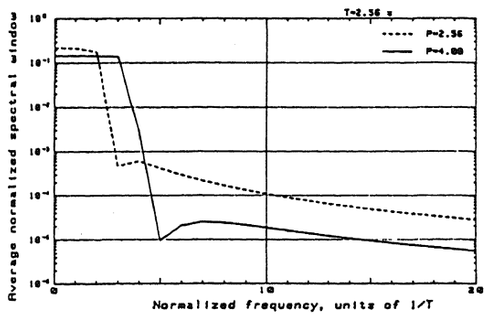

Figure 4. Average normalized spectral windows calculated from a set of data windows shown in Fig.3(a) (solid line) and Fig.3(b) (dotted line).

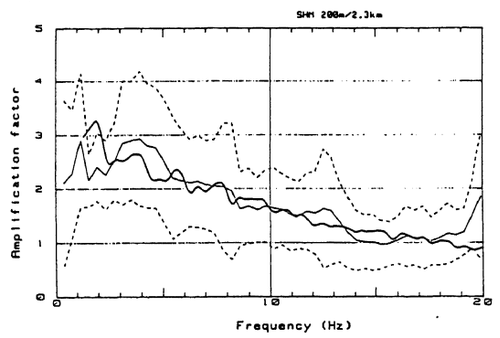

Figure 5. Amplification factors of $G_1(\lambda)$: estimated average amplification factor (real line) and calculated gain (bold line). The calculation is made assuming an incidence angle of 30° at the 2.3 km depth point and $1/Q(\omega) = 1/110$. Two dotted lines indicate one standard error range.

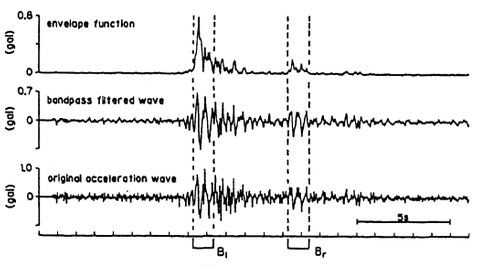

Figure 6. An example of wave segment selection. The calculations of $G_2(\lambda)$ are made from time series in the segments denoted by B_l and B_r, respectively.

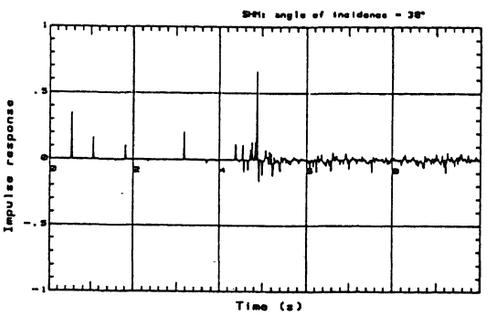

Figure 7. Impulse response of $1+\underline{X}_{p\cdot 1}(\lambda)/\overline{X}_{p\cdot 1}(\lambda)$. The calculation is made assuming an incidence angle of 30° at the 2.3 km depth point.

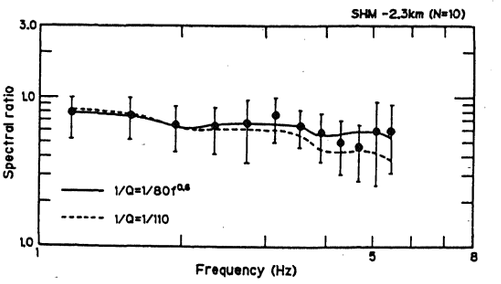

Figure 8. Estimated average spectral ratio of surface reflected pulse to the incident pulse in the basement (solid circles). Two spectral ratios are calculated by assuming $1/Q(\omega) = 1/80f^{0.6}$ (real line) and 1/110 (dotted line). In both cases, the calculation is made assuming an incidence angle of 30° at the 2.3 km depth point.

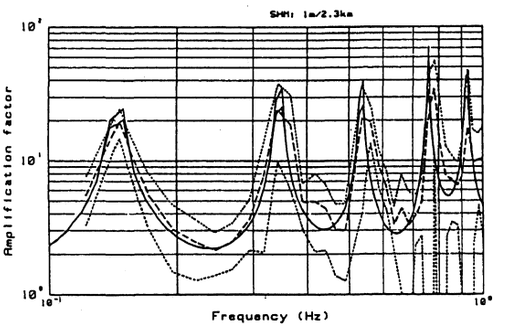

Figure 9. Estimated average amplification factor of $G_3(\lambda)$ (dashed line). Two dotted lines indicate one standard error range and two real lines are gains of $G_3(\lambda)$ calculated assuming the same incidence angle of 30° at the 2.3 km depth point and $1/Q(\omega) = 1/60f^{0.5}$ and $= 1/110$.